Advanced Characterization of Oxide Traps: The Dynamic Time-Dependent Defect Spectroscopy

T. Grasser, K. Rott•, H. Reisinger•, P.-J. Wagner*, W. Goes*, F. Schanovsky*, M. Waltl*, M. Toledano-Luque°, and B. Kaczer°*

* Institute for Microelectronics, TU Wien, Austria • Infineon, Munich, Germany ° imec, Leuven, Belgium

***Abstract*— An accurate understanding of oxide traps is essential for a number of reliability issues, including the bias temperature instability, hot carrier degradation, time-dependent dielectric breakdown, random telegraph and 1/f noise. Recent results have demonstrated that hole capture and emission into oxide traps in pMOS transistors are more complicated than the usually assumed Shockley-Read-Hall-like process. In particular, both charging and discharging proceed via a non-radiative multiphonon (NMP) mechanism involving metastable defect states. The existence of these metastable states can be demonstrated by extending the previously introduced time-dependent defect spectroscopy (TDDS) to a more general dynamic case by employing AC stresses and precisely timed discharge pulses during recovery. Application of AC stresses clearly reveals a frequency-dependence of the effective capture time, which confirms the existence of an intermediate metastable state. Application of pulses during recovery, on the other hand, allows extraction of the effective emission time also in depletion as well as in accumulation, thereby clearly revealing a metastable switching state. While all investigated traps show a frequency-dependent capture time constant, suggesting them to be of the same microscopic origin, we find two different kinds of emission behavior, namely fixed positive and switching traps. We finally demonstrate that our multi-state NMP model perfectly captures both cases.**

I. Introduction

The effective capture and emission times, τ_c and τ_e, of oxide defects have conventionally been studied via the analysis of random telegraph noise (RTN). This method analyzes the fluctuations around the equilibrium occupancy of the traps at a certain bias and works best when capture and emission times are of the same order of magnitude. Typically, τ_c and τ_e can be resolved over 3 orders of magnitude over a gate voltage range of 200 mV (in thin oxides) [1–3]. As we have demonstrated [4], this limited measurement window does not even begin to reveal the rich features of τ_c and τ_e over the whole operating regime of the transistor.

By switching the gate voltage, dynamic transitions between the old and the new equilibrium occupancy can be studied. This fact has been exploited in the recently introduced time-dependent defect spectroscopy (TDDS) [4, 5], which is a individual-trap variant of the deep-level transient spectroscopy (DLTS) [6, 7]. Up to now we have predominantly used constant voltages during the charging and discharging phases [5, 8–10]. These experiments have revealed the following schematic model for the dominant defects in the oxide of SiON pMOSFETs (see Fig. 1):

- Defects can be either fixed positive or switching traps, consistent with previous studies on large-area devices [11–13]. This implies and confirms the existence of a neutral metastable state (1' in our notation).

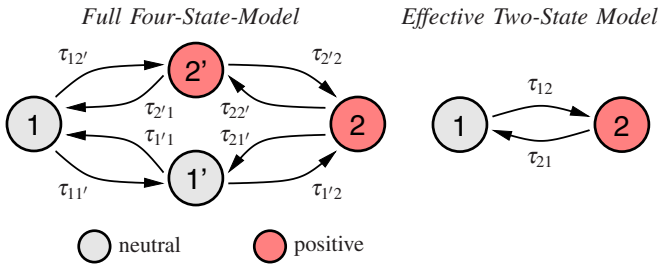

Fig. 1. **Left**: The four states of oxide defects extracted from DC TDDS experiments [4]. Each defect has two stable states, 1 and 2, and possibly two metastable states 1' and 2'. The metastable state 2' seems to be always present, while the existence of the metastable state 1' decides on whether the trap behaves like a fixed positive or a switching trap [11, 12]. **Right**: An effective two-state approximation of the four-state defect using the first-passage times τ_{12} and τ_{21} [4, 17].

- The capture times are strongly bias dependent, consistent with previous RTN studies [1, 2]. However, for very large oxide fields, a saturation behavior is observed.
- The capture and emission times of individual defects appear de-correlated. This suggests that charging proceeds via a metastable state 2'.

In our initial study [4] we have introduced the metastable state 2' and described the transitions $1 \rightleftarrows 2'$ using a conventional non-radiative multiphonon (NMP) model [1, 14–16], while the transitions $2' \rightleftarrows 2$ were modeled using a simple relaxation over a thermal barrier. Using these conventional models, the metastable state 2' introduces both a saturation in τ_c (when $\tau_{2'2}$ becomes the dominant time constant due to the strong bias dependence of $\tau_{12'}$ and $\tau_{2'1}$) as well as a de-correlation of the effective times $\tau_c = \tau_{12}$ and $\tau_e = \tau_{21}$, which are given by the respective first-passage times [17]. While both experimental observations provide strong evidence for state 2', they do not rule out alternative explanations via an (hitherto unknown) charging/discharging mechanism different to the assumed non-radiative multiphonon mechanism.

We remark that the multistate model of Fig. 1 agrees in many ways with properties previously ascribed to E' centers [11, 12, 18], in particular the metastable switching configuration 1' and the existence of a non-puckered vs. puckered configuration (possibly 2' and 2) [19]. However, density functional theory calculations in bulk SiO_2 [20, 21] do not give thermodynamic energy levels and barriers fully consistent with our electrical data [21, 22]. Whether this is due to the influence of additional strain or the amorphous nature at the interface, or other limiting assumptions in the model calculations is unclear at the moment and the identification of the microscopic nature of these oxide defects requires further work [23].

978-1-4799-0113-5/13/$31.00 ©2013 IEEE

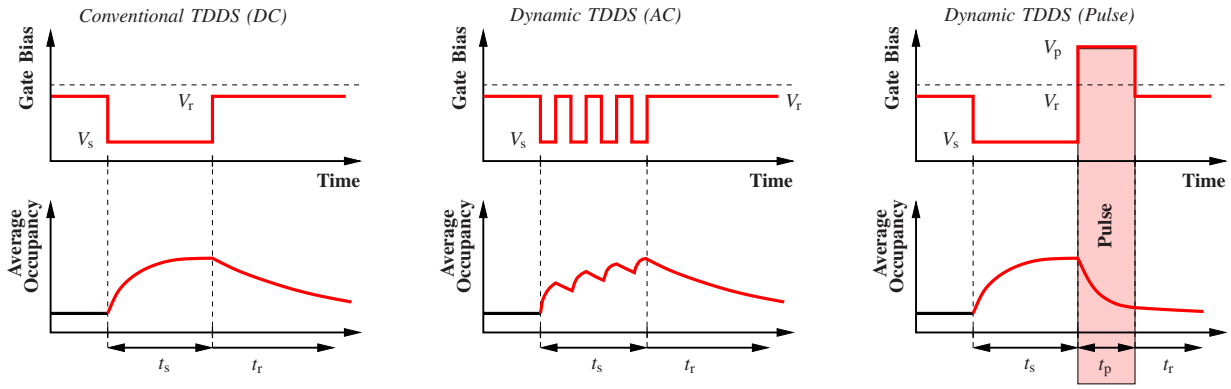

Fig. 2. **Left**: In the conventional DC TDDS measurement, defects are charged at a stress voltage V_s and discharged during the subsequent recovery at V_r. This sequence is typically repeated 100 times to allow for a statistical analysis of the discrete emission events. **Middle**: In the dynamic AC TDDS measurement, defects are subjected to an AC signal switching between V_s and V_r, followed by a discharge period at V_r. **Right**: In the dynamic pulse TDDS, a pulse V_p is applied for the duration t_p between the charging and discharging biases. Depending on the value of the emission time constant at V_p, the occupancy can be significantly reduced compared to what is obtained after the pure DC pulse. In the simplest case, the occupancy follows $\exp(-t_p/\tau_p)$, which can be used to extract τ_e over a wide range of V_p.

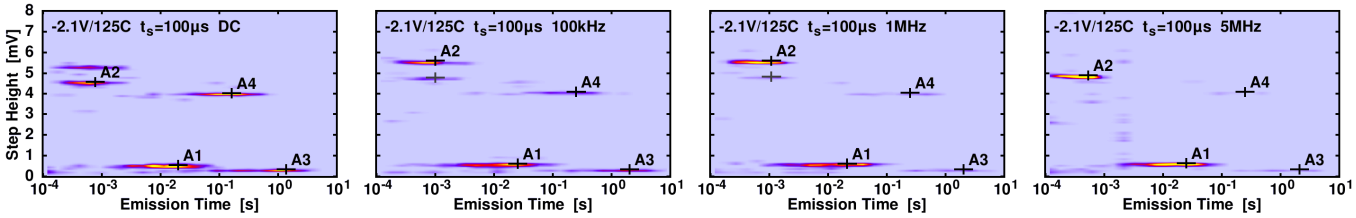

Fig. 3. Some selected experimental DC and AC TDDS spectral maps, demonstrating the f dependence of τ_c. As predicted by the four-state defect theory [24, 25], hole capture is delayed under AC conditions compared to DC (**left**). With increasing frequency, the capture time constants of defects A3 and A4 increase, visible by their clusters in the spectral map becoming fainter. As defects A1 and A2 have capture times shorter than $10\,\mu s$ at the two temperatures considered here, any potential frequency dependence could not be resolved.

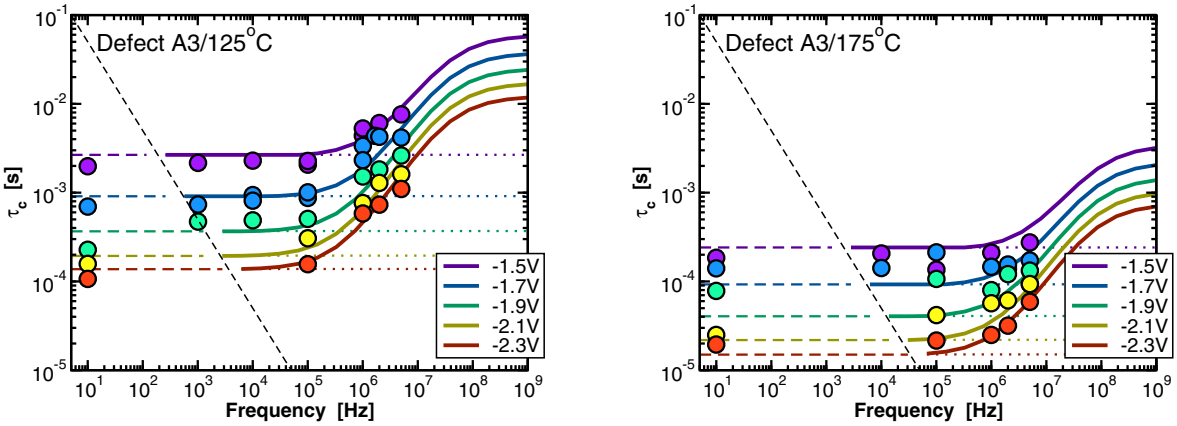

Fig. 4. Comparison of model (lines) and data (symbols) for the bias dependence of τ_c of defect A3 under AC conditions as a function of f at 125 °C (**left**) and 175 °C (**right**). For f larger than a critical frequency f_c about 100 kHz, τ_c increases until it reaches a saturation level. For the conventional first-order (two-state) model, no f dependence is obtained (dotted lines). The dashed lines show the minimum f possible experimentally, given by the requirement that τ_c has to be larger than one half period of the AC signal.

In the following the existence of both metastable states 1' and 2' as well as the physical processes responsible for the various transitions between them will be studied using an extended TDDS setup, see Fig. 2. A considerable amount of revealing data can be produced by replacing the DC stress period of the conventional TDDS setup by an AC stress [25–29] or by inserting controlled pulses into the recovery phase.

II. The AC TDDS

In a decisive experiment to confirm the existence of state 2', the DC stress phase of the TDDS setup was replaced by an AC stress, see Fig. 2 [25, 26]. Although the two-state approximation is designed to have the same expectation values for the capture and emission times under DC conditions [17], it is fundamentally different under AC conditions because it has a *frequency-independent* effective capture time τ_c [26, 30, 31]. The full four-state model, on the other hand, where only the pathway $1 \rightleftarrows 2' \rightarrow 2$ is relevant during stress (making it essentially a three-state model), can result in a *frequency-dependent* effective τ_c [24]. This overall frequency-dependence can be weaker or stronger, depending on the values of the four time constants $\tau_{12'}$, $\tau_{2'1}$, $\tau_{2'2}$ and $\tau_{22'}$. Since these time constants depend on bias and temperature, the

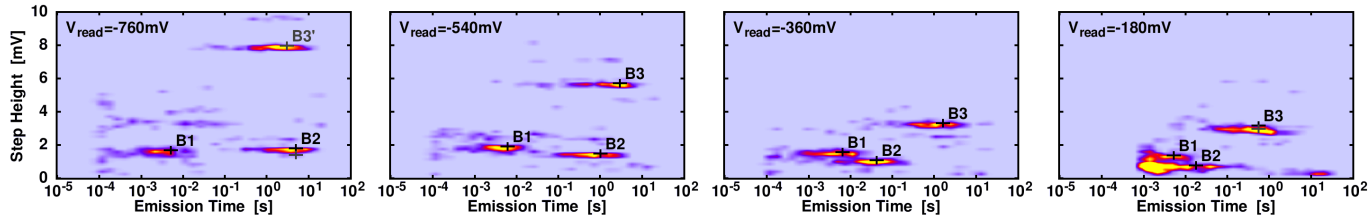

Fig. 5. Spectral maps of the DC TDDS at different readout (recovery) voltages demonstrating the resolution limit of the method. With decreasing readout voltage, the effective emission time constants of the switching traps B2 and B3 decrease, with B2 being much more sensitive than B3. On the other hand, τ_e of the simple trap B1 stays constant. Also, for these defects, the step-heights become smaller with decreasing readout voltage, resulting in overlapping defect clusters compared to the left-most figure. Furthermore, the lower the readout voltage, the lower the drain current becomes, which results in larger response times of the equipment, thereby limiting the resolution. In particular, a readout voltage of $-180\,\mathrm{mV}$ (rightmost spectral map) is very close to the resolution limit for B1.

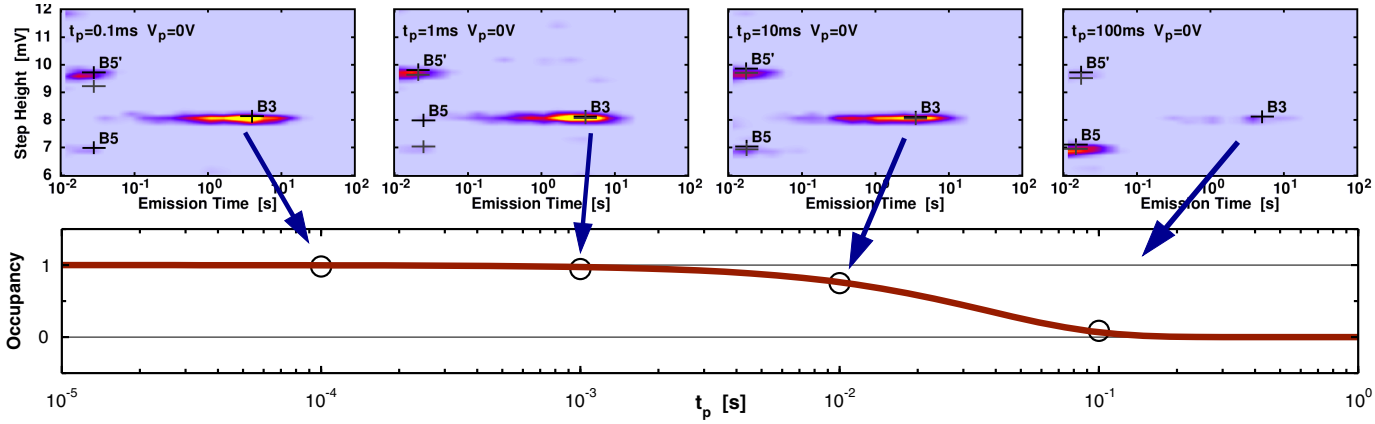

Fig. 6. **Top**: Occupancy of defect B3 in the spectral map for increasing pulse time t_p at $V_p = 0\,\mathrm{V}$. With increasing t_p, the occupancy decreases as the defect is more and more discharged at V_p. **Bottom**: As expected, the experimental occupancy (symbols) follows $\exp(-t_p/\tau_p)$ (line), which allows one to extract $\tau_e(0\,\mathrm{V}) = 40\,\mathrm{ms}$. Note also defect B5, which appeared after 3 weeks of measuring on this device and was not visible in the initial spectral map shown in Fig. 5. A correlation analysis shows [4] that when B3 is charged, the step-height of B5 increases from 7 to 9.8 mV. On the other hand, defect B2 of Fig. 5 disappeared after two weeks.

frequency-dependence is also bias and temperature dependent. However, these time constants also describe the DC features of the model, namely the bias and temperature dependence of τ_c and τ_e. As such, if state 2' exists and the model is correct, it must be able to describe τ_c and τ_e under both DC and AC conditions as a function of temperature and bias. In other words, since no new parameters are introduced in the four-state model, both DC and AC conditions must be captured by the same parameter set. Dynamic AC TDDS experiments have confirmed that this is indeed the case [25]. For example, Fig. 3 shows how the occupancy of the traps in the spectral map decreases with increasing frequency. Furthermore, Fig. 4 demonstrates that the defect model accurately captures this frequency-dependence as a function of bias and temperature.

III. The Recovery-Pulse TDDS

While charging follows the pathway $1 \rightleftarrows 2' \rightarrow 2$, discharge may proceed either via $2'$ or $1'$. The latter route becomes relevant when the defect level E_T' (the switching level, details in [4]) moves below the Fermi-level of the substrate. Then, the previously charged defect is neutralized ($2 \rightarrow 1'$). The duration of this transition is determined by $\tau_{21'}$, which will have become smaller than the bias-independent $\tau_{22'}$ under these conditions.

Regarding the discharge of the defects it has been observed that some defects, the so-called switching traps, are sensitive to the gate bias [11, 12], while others are not. From a reliability standpoint, it has been demonstrated that the recoverable component of NBTI, which has been linked to such oxide traps [32–36] is highly sensitive to switches into the depletion regime [37–39]. However, the DC TDDS requires a certain current flow through the transistors and τ_e cannot be completely studied in depletion to better understand and link the behavior of individual traps to NBTI, see Fig. 5. By introducing a well controlled discharge pulse right after stress, we extend the TDDS to allow for the extraction of τ_e throughout the whole depletion and even into the accumulation regimes of the transistor.

The idea of this recovery-pulse TDDS is simple: suppose that we apply a certain stress/charging pulse V_s of duration t_s, followed by a discharge period at V_r. Assuming for simplicity that in equilibrium at V_s the defect becomes fully charged ($f_2 = 1$), while during relaxation at V_r it becomes completely discharged ($f_2 = 0$), the expectation value of the occupancy is given by [17]

$$f_2 = \big(1 - \exp(-t_s/\tau_c)\big)\exp(-t_r/\tau_e). \qquad (1)$$

State 2 is here the stable positive state of the multi-state defect model, see Fig. 1. If we now insert a pulse of duration t_p at a voltage V_p, we have with $\tau_p = \tau_e(V_p)$ and for $|V_p| < |V_r|$

$$f_2 = \big(1 - \exp(-t_s/\tau_c)\big)\underbrace{\exp(-t_p/\tau_p)}_{\text{Impact of Pulse}}\exp(-t_r/\tau_e). \qquad (2)$$

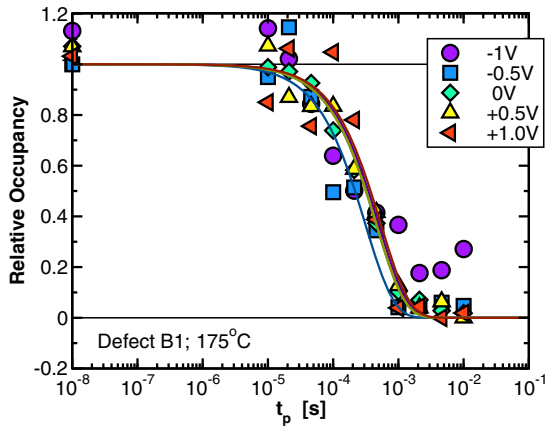

Fig. 7. Experimental relative occupancy (symbols) of defect B1 as a function of the pulse duration t_p for various values of the pulse voltage V_p. The fits of the data to $\exp(-t_p/\tau_e(V_p))$ are given by the lines, which show no pulse bias dependence of $\tau_e(V_p) \sim$ const. The DC TDDS value ($t_p = 0$s) is shown at $t_p = 10$ns. Occupancies larger than 1 are caused by extraction errors due to noise (cf. Fig. 5).

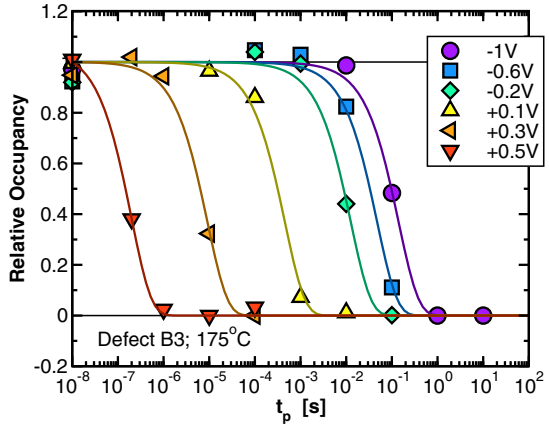

Fig. 8. Same as Fig. 7 but for the switching trap B3. Clearly, a very strong sensitivity to the pulse bias V_p is observed. The noise level in the extraction (uncertainty in step-height detection) is much better for defect B3 compared to B1, as can also be seen in Fig. 5. Thus, for every V_p only four values of t_p were used for the extraction.

Naturally, if $t_p \gg \tau_p$, the defect will completely disappear from the map. On the other hand, for $t_p \ll \tau_p$, the occupancy will not be affected. However, by choosing $t_p \approx \tau_p$, the differences in f_2 between eq. (2) and eq. (1) allow us to extract τ_p. Since extraction of f_2 via the spectral map of the TDDS requires many repetitions of the basic charging/discharging sequence shown in Fig. 2 for accurate statistics and since τ_p is not known *a priori*, it appears more reliable to chose a few values of t_p around the expected τ_p and fit the data to eq. (2), which is essentially the $\exp(-t_p/\tau_p)$ term.

A. Proof of Concept

The basic features of the dynamic TDDS are demonstrated in Fig. 6. In our previous TDDS studies we had been using a single device for a duration of about three years [4, 5, 25], which unfortunately was destroyed by a handling accident unrelated to the actual experiments during the course of this

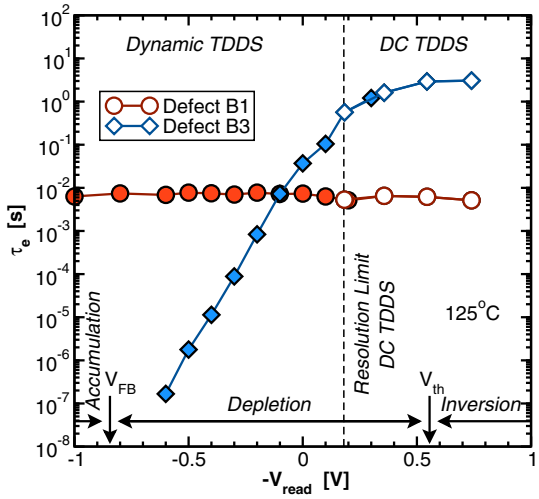

Fig. 9. A comparison of the extracted emission times obtained by the DC (open symbols) and the dynamic recovery-pulse TDDS (filled symbols) for defects B1 and B3. Not only does the recovery-pulse TDDS deliver consistent results with the DC TDDS, it allows one to extract τ_e down from inversion, through depletion and even into the accumulation region.

study. In the following, defects belonging to this initial device have the prefix A (see Fig. 3 and Fig. 4), while the recovery-pulse TDDS experiments were performed on a new device, B. Based on the same setup as used in the DC TDDS of the leftmost panel in Fig. 5, we introduce a pulse from V_r down to $V_p = 0$V for $t_p = 100\,\mu$s, 1ms, 10ms, and 100ms. Clearly, the occupancy of defect B3 is reduced with increasing t_p. When the occupancies extracted from the spectral maps are plotted as a function of t_p, good agreement with the theoretical $\exp(-t_p/\tau_p)$ dependence is obtained, allowing for the extraction of $\tau_e(0\,\text{V}) = 40$ms.

The recovery-pulse TDDS is now applied to study the bias dependence of τ_e for the defects B1 and B3. Unfortunately, B2 disappeared after two weeks of measurements, similarly to A6 in our previous study [4], implying another possible defect transformation [13, 36, 40–42]. The dependence of the occupancy f_2 for a few selected values of V_p is shown in Fig. 7 and Fig. 8. As can be seen, τ_e of defect B1 remains at a bias-independent value of about 0.4ms throughout depletion and into accumulation. On the other hand, τ_e of B3 depends exponentially on the bias in depletion, continuing the trend already observable in Fig. 5.

A comparison of τ_e obtained by the DC and recovery-pulse TDDS is given in Fig. 9. Both methods deliver the same result in the region where the DC TDDS can be applied, while the recovery-pulse TDDS works well into the depletion regime and even into accumulation. The exceptional resolution of the recovery-pulse TDDS is clearly seen, allowing us in this case to extract τ_e over 6 orders of magnitude for defect B3. From a practical viewpoint, the DC TDDS has already been used to extract values of τ_e of up to 1ks, giving the recovery-pulse TDDS an unparalleled resolution of 10 orders of magnitude. As such, the whole operating regime of the transistor can be covered, allowing us to extract values of τ_e and τ_c from accumulation into strong inversion.

Here it has to be noted that, roughly speaking, the TDDS gives best results for the *shorter* of the two time constants, as this time constant dominates the transition between the equilibrium states [17]. To be more precise on this somewhat subtle issue consider for example a two-state defect. The expectation value of the defect occupancy during a transition between states 1 and 2 is given by

$$f(t_s) = f^H + (f^L - f^H)\,e^{-t_s/\tau}$$

with

$$f^L = \frac{\tau_e^L}{\tau_e^L + \tau_c^L}, \quad f^H = \frac{\tau_e^H}{\tau_e^H + \tau_c^H}, \quad \text{and} \quad \frac{1}{\tau} = \frac{1}{\tau_c^H} + \frac{1}{\tau_e^H},$$

where the superscripts L and H denote the values at the recovery and stress voltage, respectively. Usually, as also assumed in eq. (1), $f^L = 0$, $f^H = 1$, and $\tau = \tau_c^H$. For low stress voltages or high recovery voltages, however, this is no longer the case. Since the TDDS uses the occupancy of the defect during stress to calculate the capture time constant, it actually determines the decorrelation time τ rather than τ_c. During emission, on the other hand, the statistics of the first emission event are recorded, which corresponds to τ_e. Finally, the recovery-pulse TDDS also monitors the occupancy in the spectral map to calculate the emission time at a different bias, so it also determines τ rather than τ_e. However, for typical bias conditions such as those shown in Fig. 9 we have $\tau \approx \tau_e$. As such, the TDDS is considerably simpler when one of the time constants dominates.

For the three-state defect (assuming the transition via 2' to be dominant), the TDDS extracts the first passage time for the transition $2 \rightarrow 1$ (the average emission time)

$$\tau_e = \frac{k_{2'2} + k_{22'} + k_{2'1}}{k_{22'}\ k_{2'1}} \tag{3}$$

since it again analyzes the first step in the emission transient. Extraction of the capture time proceeds via the occupancy in the spectral map, which is given by the effective time constant of the system (the decorrelation time)

$$\tau = \frac{k_{12'} + k_{2'1} + k_{2'2} + k_{22'}}{k_{22'}\ k_{2'1} + k_{12'}(k_{22'} + k_{2'2})} \tag{4}$$

assuming that the pathway 2' is dominant. For sufficiently large bias, the time constant corresponds to the first passage time for the transition $1 \rightarrow 2$ (the average capture time)

$$\tau_c = \frac{k_{12'} + k_{2'1} + k_{2'2}}{k_{12'}\ k_{2'2}}. \tag{5}$$

Note that eq. (4) simplifies to eq. (3) for lower biases. Finally, since the recovery-pulse TDDS also monitors the occupancy, it in principle also extracts τ, which, however, is equivalent to τ_e for low enough biases.

B. Theory

Using the recovery-pulse TDDS, the time constants for defect B1 and B3 have been extracted from accumulation to strong inversion at 125 °C and 175 °C and fitted by the multi-state NMP model. The highly satisfactory results for defect B1 are shown in Fig. 10. Higher stress voltages than 2.5 V were omitted for this 2.2 nm oxide [44] in order to avoid oxide breakdown, but pose otherwise no limitation to the TDDS. As noted before, B1 has a bias-independent τ_e, meaning that the neutral metastable switching state 1' is not accessible, as shown in the configuration coordinate and state diagrams of Fig. 11. As such, recovery proceeds from the stable positive state 2 to the neutral stable state 1 via the pathway 2→2'→1. In other words, discharging follows the opposite route as charging.

On the other hand, in the switching trap B3, the metastable state 1' is accessible, leading to an exponential bias dependence of τ_e below the threshold voltage well into depletion, see Fig. 12, closely tracking the surface hole concentration. In this regime, discharge takes the alternative pathway 2→1'→1, while (roughly) above the threshold voltage the conventional pathway 2→2'→1 is followed, see Fig. 13. For low enough biases, recovery is then accelerated by the large surface

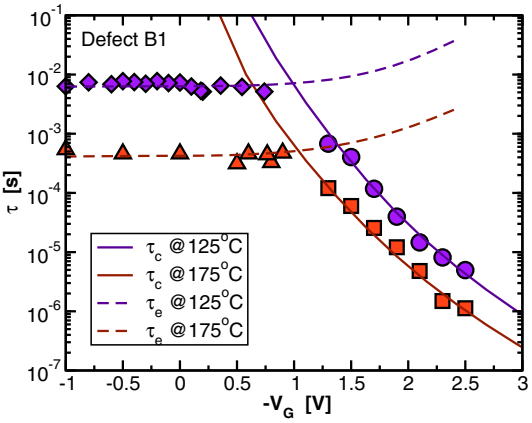

Fig. 10. The capture and emission times of the simple defect B1 at two temperatures. The symbols are the data while the lines are from the NMP model of Fig. 11. Excellent agreement between theory and data is obtained.

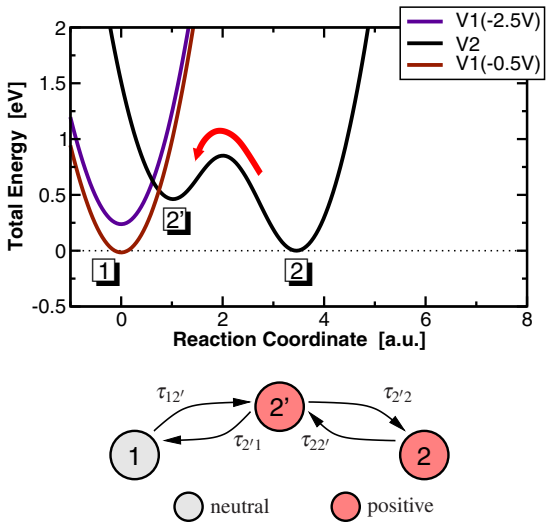

Fig. 11. Configuration coordinate diagram [4, 17, 43] of the NMP model for two bias conditions (top) and state diagram (bottom) of the simple defect B1. The metastable state 1', responsible for the switching trap behavior is not accessible, leading to bias-independent recovery via the sequence 2→2'→1.

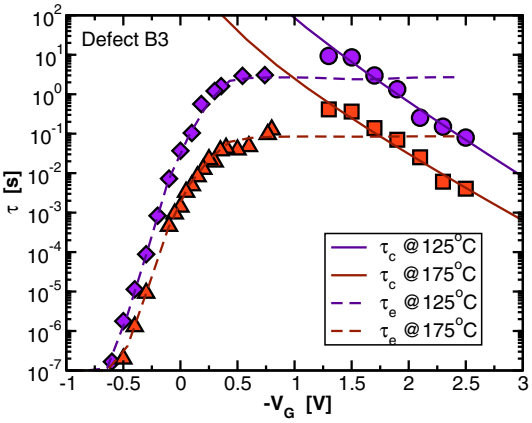

Fig. 12. The capture and emission times of switching trap B3 at two temperatures. The symbols are the data while the lines are from the NMP model of Fig. 13. Excellent agreement between theory and data is obtained over 8 orders of magnitude.

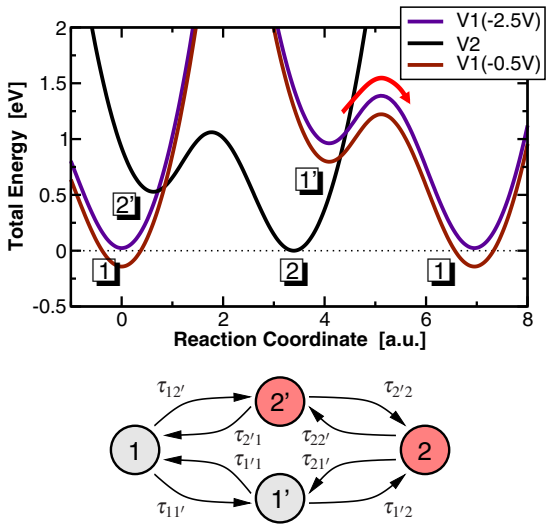

Fig. 13. Configuration coordinate and state diagrams just as in Fig. 11, but for the switching trap B3. Contrary to defect B1, the metastable state 1' is accessible, leading to strongly bias-dependent recovery via the sequence 2→1'→1 at more positive gate bias.

electron concentration. Just like with defect B1, the NMP model gives a perfect match to the experimental data, thereby strongly supporting its validity.

IV. Conclusions

We have extended the recently suggested time-dependent defect spectroscopy (TDDS) to a more dynamic case by using AC stresses and controlled pulses right after the charging sequence. In this dynamic TDDS, the metastable defects can be probed in a detailed manner. In particular, AC stresses reveal an intermediate metastable defect state, which is part of the charging sequence and introduces a strong frequency dependence. On the other hand, application of controlled pulses allows us to probe the emission times of the defects both in depletion as well as in accumulation. While the metastable state seems to be always present during capture, two types of defects are observed, which appear to occur with (very roughly) similar densities: simple defects, which do not show a bias-dependence of τ_e, and switching traps, which show an exponential bias-dependence. These results consistently explain why a positive pulse after NBTI stress does not necessarily remove all trapped charges in the oxide to unearth the 'permanent' part [45]. Using the recovery-pulse TDDS, the effective defect time constants can be extracted over 10 orders of magnitude from accumulation to strong inversion, providing an unparalleled resolution. Finally, we have demonstrated that the previously suggested multi-state NMP model accurately describes and explains the experimental behavior.

V. Acknowledgments

The research leading to these results has received funding from the FWF project n°23390-M24 and the European Community's FP7 project n°261868 (MORDRED)

References

[1] A. Palma, A. Godoy, J. A. Jimenez-Tejada, J. E. Carceller, and J. A. Lopez-Villanueva, "Quantum Two-Dimensional Calculation of Time Constants of Random Telegraph Signals in Metal-Oxide-Semiconductor Structures," *Physical Review B*, vol. 56, no. 15, pp. 9565–9574, 1997.

[2] N. Zanolla, D. Siprak, P. Baumgartner, E. Sangiorgi, and C. Fiegna, "Measurement and Simulation of Gate Voltage Dependence of RTS Emission and Capture Time Constants in MOSFETs," in *Proc. Workshop on Ultimate Integration of Silicon*, Udine, Italy, Mar. 2008, pp. 137–140.

[3] J. Campbell, J. Qin, K. Cheung, L. Yu, J. Suehle, A. Oates, and K. Sheng, "Random Telegraph Noise in Highly Scales nMOSFETs," in *Proc. Intl.Rel.Phys.Symp. (IRPS)*, 2009, pp. 382–388.

[4] T. Grasser, H. Reisinger, P.-J. Wagner, W. Goes, F. Schanovsky, and B. Kaczer, "The Time Dependent Defect Spectroscopy (TDDS) for the Characterization of the Bias Temperature Instability," in *Proc. Intl.Rel.Phys.Symp. (IRPS)*, May 2010, pp. 16–25.

[5] T. Grasser, H. Reisinger, P.-J. Wagner, and B. Kaczer, "The Time Dependent Defect Spectroscopy for the Characterization of Border Traps in Metal-Oxide-Semiconductor Transistors," *Physical Review B*, vol. 82, no. 24, p. 245318, 2010.

[6] D. Lang, "Deep-Level Transient Spectroscopy: A New Method to Characterize Traps in Semiconductors," *J.Appl.Phys.*, vol. 45, no. 7, pp. 3023–3032, 1974.

[7] A. Karwath and M. Schulz, "Deep Level Transient Spectroscopy on Single, Isolated Interface Traps in Field-Effect Transistors," *Appl.Phys.Lett.*, vol. 52, no. 8, pp. 634–636, 1988.

[8] H. Reisinger, T. Grasser, and C. Schlünder, "A Study of NBTI by the Statistical Analysis of the Properties of Individual Defects in pMOSFETs," in *Proc. Intl.Integrated Reliability Workshop*, 2009, pp. 30–35.

[9] H. Reisinger, T. Grasser, W. Gustin, and C. Schlünder, "The Statistical Analysis of Individual Defects Constituting NBTI and its Implications for Modeling DC- and AC-Stress," in *Proc. Intl.Rel.Phys.Symp. (IRPS)*, May 2010, pp. 7–15.

[10] M. Toledano-Luque, B. Kaczer, P. J. Roussel, M. Cho, T. Grasser, and G. Groeseneken, "Temperature Dependence of the Emission and Capture Times of SiON Individual Traps after Positive Bias Temperature Stress," *J.Vac.Sci.Technol.B*, vol. 29, pp. 01AA04–1–01AA04–5, 2011.

[11] A. Lelis and T. Oldham, "Time Dependence of Switching Oxide Traps," *IEEE Trans.Nucl.Sci.*, vol. 41, no. 6, pp. 1835–1843, Dec 1994.

[12] J. Conley Jr., P. Lenahan, A. Lelis, and T. Oldham, "Electron Spin Resonance Evidence that E'_γ Centers can Behave as Switching Oxide Traps," *IEEE Trans.Nucl.Sci.*, vol. 42, no. 6, pp. 1744–1749, 1995.

[13] T. Grasser, B. Kaczer, W. Goes, T. Aichinger, P. Hehenberger, and M. Nelhiebel, "Understanding Negative Bias Temperature Instability in the Context of Hole Trapping," *Microelectronic Engineering*, vol. 86, no. 7-9, pp. 1876–1882, 2009.

[14] K. Huang and A. Rhys, "Theory of Light Absorption and Non-Radiative Transitions in F-Centres," *Proc.R.Soc.A*, vol. 204, pp. 406–423, 1950.

[15] C. Henry and D. Lang, "Nonradiative Capture and Recombination by Multiphonon Emission in GaAs and GaP," *Physical Review B*, vol. 15, no. 2, pp. 989–1016, 1977.

[16] W. Fowler, J. Rudra, M. Zvanut, and F. Feigl, "Hysteresis and Franck-Condon Relaxation in Insulator-Semiconductor Tunneling," *Physical Review B*, vol. 41, no. 12, pp. 8313–8317, 1990.

[17] T. Grasser, "Stochastic Charge Trapping in Oxides: From Random Telegraph Noise to Bias Temperature Instabilities," in *Microelectronics Reliability*, vol. 52, 2012, pp. 39–70.

[18] E. Poindexter and W. Warren, "Paramagnetic Point Defects in Amorphous Thin Films of SiO_2 and Si_3N_4: Updates and Additions," *J.Electrochem.Soc.*, vol. 142, no. 7, pp. 2508–2516, 1995.

[19] A. Kimmel, P. Sushko, A. Shluger, and G. Bersuker, "Positive and Negative Oxygen Vacancies in Amorphous Silica," in *Silicon Nitride, Silicon Dioxide, and Emerging Dielectrics 10*, R. Sah, J. Zhang, Y. Kamakura, M. Deen, and J. Yota, Eds. ECS Transactions, 2009, vol. 19, pp. 2–17.

[20] P. Blöchl, "First-Principles Calculations of Defects in Oxygen-Deficient Silica Exposed to Hydrogen," *Physical Review B*, vol. 62, no. 10, pp. 6158–6179, 2000.

[21] F. Schanovsky, W. Goes, and T. Grasser, "Multiphonon Hole Trapping from First Principles," *J.Vac.Sci.Technol.B*, vol. 29, no. 1, pp. 01A2011–01A2015, 2011.

[22] T. Grasser, B. Kaczer, W. Goes, H. Reisinger, T. Aichinger, P. Hehenberger, P.-J. Wagner, F. Schanovsky, J. Franco, M. Toledano-Luque, and M. Nelhiebel, "The Paradigm Shift in Understanding the Bias Temperature Instability: From Reaction-Diffusion to Switching Oxide Traps," *IEEE Trans.Electron Devices*, vol. 58, no. 11, pp. 3652–3666, 2011.

[23] J. Ryan, P. Lenahan, T. Grasser, and H. Enichlmair, "Recovery-Free Electron Spin Resonance Observations of NBTI Degradation," in *Proc. Intl.Rel.Phys.Symp. (IRPS)*, 2010, pp. 43–49.

[24] T. Grasser, B. Kaczer, H. Reisinger, P.-J. Wagner, and M. Toledano-Luque, "On the Frequency Dependence of the Bias Temperature Instability," in *Proc. Intl.Rel.Phys.Symp. (IRPS)*, Apr. 2012, pp. XT.8.1–XT.8.7.

[25] T. Grasser, H. Reisinger, K. Rott, M. Toledano-Luque, and B. Kaczer, "On the Microscopic Origin of the Frequency Dependence of Hole Trapping in pMOSFETs," in *Proc. Intl.Electron Devices Meeting (IEDM)*, Dec. 2012, pp. 19.6.1–19.6.4.

[26] M. Toledano-Luque, B. Kaczer, P. Roussel, T. Grasser, G. Wirth, J. Franco, C. Vrancken, N. Horiguchi, and G. Groeseneken, "Response of a Single Trap to AC Negative Bias Temperature Stress," in *Proc. Intl.Rel.Phys.Symp. (IRPS)*, 2011, pp. 364–371.

[27] K. Zhao, J. Stathis, B. Linder, E. Cartier, and A. Kerber, "PBTI Under Dynamic Stress: From a Single Defect Point of View," in *Proc. Intl.Rel.Phys.Symp. (IRPS)*, Apr. 2011, pp. 372–380.

[28] J. Zou, J. Zou, C. Liu, R. Wang, X. Xu, J. Liu, H. Wu, Y. Wang, and R. Huang, "On the Statistical Trap-Response (STR) Method for Characterizing Random Trap Occupancy and NBTI Fluctuation," in *IEEE Silicon Nanoelectronics Workshop (SNW)*, Jun. 2012, pp. 1–2.

[29] J. Zou, R. Wang, N. Gong, R. Huang, X. Xu, J. Ou, C. Liu, J. Wang, J. Liu, J. Wu, S. Yu, P. Ren, H. Wu, S. Lee, and Y. Wang, "New Insights into AC RTN in Scaled High-κ/Metal-gate MOSFETs under Digital Circuit Operations," in *IEEE Symposium on VLSI Technology Digest of Technical Papers*, 2012, pp. 139–140.

[30] C. Shen, M.-F. Li, H. Yu, X. Wang, Y.-C. Yeo, D. Chan, and D.-L. Kwong, "Physical Model for Frequency-Dependent Dynamic Charge Trapping in Metaloxide-Semiconductor Field Effect Transistors with HfO_2 Gate Dielectric," *Appl.Phys.Lett.*, vol. 86, p. 093510, 2005.

[31] H. Reisinger, T. Grasser, K. Ermisch, H. Nielen, W. Gustin, and C. Schlünder, "Understanding and Modeling AC BTI," in *Proc. Intl.Rel.Phys.Symp. (IRPS)*, Apr. 2011, pp. 597–604.

[32] V. Huard, M. Denais, and C. Parthasarathy, "NBTI Degradation: From Physical Mechanisms to Modelling," *Microelectronics Reliability*, vol. 46, no. 1, pp. 1–23, 2006.

[33] V. Huard, "Two Independent Components Modeling for Negative Bias Temperature Instability," in *Proc. Intl.Rel.Phys.Symp. (IRPS)*, May 2010, pp. 33–42.

[34] B. Kaczer, P. Roussel, T. Grasser, and G. Groeseneken, "Statistics of Multiple Trapped Charges in the Gate Oxide of Deeply Scaled MOSFET Devices-Application to NBTI," *IEEE Electron Device Lett.*, vol. 31, no. 5, pp. 411–413, 2010.

[35] D. Ang, Z. Teo, T. Ho, and C. Ng, "Reassessing the Mechanisms of Negative-Bias Temperature Instability by Repetitive Stress/Relaxation Experiments," *IEEE Trans.Dev.Mat.Rel.*, vol. 11, no. 1, pp. 19–34, 2011.

[36] Z. Teo, A. Boo, D. Ang, and K. Leong, "On the Cyclic Threshold Voltage Shift of Dynamic Negative-Bias Temperature Instability," in *Proc. Intl.Rel.Phys.Symp. (IRPS)*, 2011, pp. 943–947.

[37] B. Kaczer, T. Grasser, P. Roussel, J. Martin-Martinez, R. O'Connor, B. O'Sullivan, and G. Groeseneken, "Ubiquitous Relaxation in BTI Stressing – New Evaluation and Insights," in *Proc. Intl.Rel.Phys.Symp. (IRPS)*, 2008, pp. 20–27.

[38] T. Aichinger, M. Nelhiebel, S. Einspieler, and T. Grasser, "Observing Two Stage Recovery of Gate Oxide Damage Created under Negative Bias Temperature Stress," *J.Appl.Phys.*, vol. 107, pp. (024 508–1)–(024 508–8), 2010.

[39] T. Aichinger, M. Nelhiebel, and T. Grasser, "Energetic Distribution of Oxide Traps Created under Negative Bias Temperature Stress and their Relation to Hydrogen," *Appl.Phys.Lett.*, vol. 96, pp. (133 511–1)–(133 511–3), 2010.

[40] T. Grasser, P.-J. Wagner, H. Reisinger, T. Aichinger, G. Pobegen, M. Nelhiebel, and B. Kaczer, "Analytic Modeling of the Bias Temperature Instability Using Capture/Emission Time Maps," in *Proc. Intl.Electron Devices Meeting (IEDM)*, Dec. 2011, pp. 27.4.1–27.4.4.

[41] Y. Gao, A. Boo, Z. Teo, and D. Ang, "On the Evolution of the Recoverable Component of the SiON, HfSiON and HfO_2 P-MOSFETs under Dynamic NBTI," in *Proc. Intl.Rel.Phys.Symp. (IRPS)*, Apr. 2011, pp. 935–940.

[42] M. Duan, J. Zhang, Z. Ji, W. Zhang, B. Kaczer, S. De Gendt, and G. Groeseneken, "Defect Loss: A New Concept for Reliability of MOSFETs," *IEEE Electron Device Lett.*, vol. 33, no. 4, pp. 480–482, 2012.

[43] M. Kirton and M. Uren, "Noise in Solid-State Microstructures: A New Perspective on Individual Defects, Interface States and Low-Frequency (1/f) Noise," *Adv.Phys.*, vol. 38, no. 4, pp. 367–486, 1989.

[44] H. Reisinger, O. Blank, W. Heinrigs, A. Mühlhoff, W. Gustin, and C. Schlünder, "Analysis of NBTI Degradation- and Recovery-Behavior Based on Ultra Fast V_{th}-Measurements," in *Proc. Intl.Rel.Phys.Symp. (IRPS)*, 2006, pp. 448–453.

[45] T. Grasser, T. Aichinger, G. Pobegen, H. Reisinger, P.-J. Wagner, J. Franco, M. Nelhiebel, and B. Kaczer, "The 'Permanent' Component of NBTI: Composition and Annealing," in *Proc. Intl.Rel.Phys.Symp. (IRPS)*, Apr. 2011, pp. 605–613.